Taylor & Francis
Taylor & Francis Group

Science and Technology of Advanced Materials: Methods

ISSN: (Print) (Online) Journal homepage: www.tandfonline.com/journals/tstm20

Linking structure and process in dendritic growth using persistent homology with energy analysis

Misato Tone, Shunsuke Sato, Sotaro Kunii, Ippei Obayashi, Yasuaki Hiraoka, Yui Ogawa, Hirokazu Fukidome, Alexandre Lira Foggiatto, Chiharu Mitsumata, Ryunsuke Nagaoka, Arpita Varadwaj, Iwao Matsuda & Masato Kotsugi

To cite this article: Misato Tone, Shunsuke Sato, Sotaro Kunii, Ippei Obayashi, Yasuaki Hiraoka, Yui Ogawa, Hirokazu Fukidome, Alexandre Lira Foggiatto, Chiharu Mitsumata, Ryunsuke Nagaoka, Arpita Varadwaj, Iwao Matsuda & Masato Kotsugi (07 Mar 2025): Linking structure and process in dendritic growth using persistent homology with energy analysis, Science and Technology of Advanced Materials: Methods, DOI: 10.1080/27660400.2025.2475735

To link to this article: https://doi.org/10.1080/27660400.2025.2475735

Publisher: Taylor & Francis & The Author(s). Published by National Institute for Materials Science in partnership with Taylor & Francis Group

Journal: *Science and Technology of Advanced Materials: Methods*

DOI: 10.1080/27660400.2025.2475735

Linking structure and process in dendritic growth using persistent homology with energy analysis

Misato Tone[a], Shunsuke Sato[a], Sotaro Kunii[a], Ippei Obayashi[b], Yasuaki Hiraoka[c], Yui Ogawa[d], Hirokazu Fukidome[e], Alexandre Lira Foggiatto[a], Chiharu Mitsumata[a,f], Ryunsuke Nagaoka[a], Arpita Varadwaj[a], Iwao Matsuda[g], Masato Kotsugi[a]*

a) Department of Material Science and Technology, Tokyo University of Science, 6-3-1, Niijuku, Katsushika, Tokyo, 125-8585, Japan
b) Center for Artificial Intelligence and Mathematical Data Science, Okayama University, 2-1-1, Tsushimanaka, Kita-ku, Okayama, 700-8530, Japan
c) Kyoto University Institute for Advanced Study, Kyoto University, Yoshida Ushinomiya-cho, Sakyo-ku, Kyoto, 606-8501, Japan
d) NTT Basic Research Laboratories, 3-1 Morinosato Wakamiya, Atsugi, Kanagawa, 243-0198 Japan
e) Research Institute of Electrical Communication, Tohoku University, 2-1-1, Katahira, Aoba-ku, Sendai, Miyagi, 980-8577, Japan
f) Graduate school of Pure and Applied Science, University of Tsukuba, 1-1-1 Tennodai, Tsukuba, 305-8577 Japan
g) Institute for Solid State Physics, The University of Tokyo, Kashiwanoha 5-1-5, Kashiwa, Chiba, 277-8581 Japan

Abstract

We present a material analysis method that links structure and process in dendritic growth using explainable machine learning approaches. We employed persistent homology (PH) to quantitatively characterize the morphology of dendritic microstructures. By using interpretable machine learning with energy analysis, we established a robust relationship between structural features and Gibbs free energy. Through a detailed analysis of how Gibbs free energy evolves with morphological changes in dendrites, we uncovered specific conditions that influence the branching of dendritic structures. Moreover, energy gradient analysis based on morphological feature provides a deeper understanding of the branching mechanisms and offers a pathway to optimize thin-film growth processes. Integrating topology and free energy enables the optimization of a range of materials from fundamental research to practical applications.

*Corresponding author: kotsugi@rs.tus.ac.jp

1. Introduction

Thin film growth processes in electric devices play a critical role in the development of applied devices across a wide spectrum, from semiconductors to communication technologies. Physical properties can vary significantly depending on microstructural features such as morphology, defects, and interfaces. For beyond-5G advancements, transistor applications like field-effect transistors and channel materials are gaining significant attention[1–6]. There is also growing interest in applications for mechatronics and IoT sensors[3,6–14]. Notably, graphene and hexagonal boron nitride (h-BN) multilayer films on copper substrates are expected to exhibit high carrier mobility, making them promising candidates for applications such as gigahertz-range photodetectors[1,8,9,12,14,15]. Extensive applications are rapidly progressing, spanning semiconductor devices, communication technologies, and sensor technologies.

To fully harness the performance of these multilayer film devices, it is crucial to precisely fabricate the Cu substrate serving as a catalyst, in addition to the graphene and borophene layers themselves. This is because the carrier density of the multilayer films strongly depends on their structural configuration, which in turn affects the functions such as absorption rate and light-harvesting efficiency [3,16,17]. Significant progress has been made in structural analyses of graphene and borophene at the atomic scale based on topological methods[15].

However, mesoscale morphological fine structures are known to be significantly influenced by process conditions such as atmosphere, composition and surface defects. Achieving large-area fabrication of these materials is a critical step toward the practical application of devices. Yet, dendritic structures that emerge during the growth process are considered major obstacles hindering large-area fabrication [8,18]. Currently, process optimization involves considerable trial and error, underscoring the need for analysis of dendrite morphology and systematic process design.

Dendritic growth is a cause that reduces the flatness of thin films, necessitating control and understanding of the growth process[19]. Dendritic structures are formed through the precipitation of complex, branched dendrites during the film growth process. Dendrites are frequently observed in materials such as Cu, graphene, and borophene, appearing extensively in early growth stage and multilayer films [7–9,17,19,20].

Experimentally, dendritic structures have been observed using microscopy; however, simple visual analysis requires substantial effort and makes it difficult to delve deeply into the growth mechanisms. Computationally, phase-field simulations have been conducted, providing precise simulations through large-scale calculations. Nevertheless, morphological analyses have been performed by simple image analyses (e.g., grain size and curvature). Particularly, analyses of complex structural morphologies and understanding of their mechanisms remain underdeveloped, with qualitative and subjective structural analyses persisting over time [16,17,21–24]. It has been challenging to clarify the conditions leading to dendritic branching that causes functional degradation, and it has been equally difficult to feed these conditions back into the process. Thereby, many missing links still exist among structure, process, and mechanism.

In this study, we employed data science approaches to establish a hierarchical connection between structure and process in dendritic growth (Fig. 1). We focused on dendrite morphology and the free energy—which is crucial in the growth process—and linked them through data-driven methods. We introduced a mathematical topology technique called persistent homology (PH) to analyze the dendrite structures, with the core idea of characterizing their morphology using homology concepts [25–30]. We attempted to investigate the growth and branching of dendritic structures and to detect the causes of their functional degradation. By employing interpretable machine learning methods and energy analysis, we robustly connected microstructural features with system stability in dendritic growth, proposing novel explainable AI models for materials design. As a pilot study, we selected hexagonal Cu, a simple and widely used substrate. We validated our analytical method using image data generated through phase-field simulations, thereby establishing the foundation of the method.

PH is a cutting-edge concept in topology that enables multiscale analysis of holes and connections within geometric structures, recently developed by Carlsson, Edelsbrunner, and Hiraoka [25–30]. PH can handle topological data across multiscale and is applicable to point cloud data such as atomic arrangements, as well as two-dimensional image data. It is particularly effective for analyzing inhomogeneous but not entirely random data, such as amorphous and porous materials[27–29]. We utilized PH to extract the morphology of dendritic structures as feature vectors.

Dendritic structures are distinguished by their hierarchical branching and intricate connectivity, setting them apart from both crystalline grains and amorphous materials. Unlike crystalline structures—characterized by periodic boundaries—or amorphous materials, which lack well-defined connectivity, dendrites develop complex, tree-like morphologies that evolve dynamically during growth. Persistent homology (PH) is particularly well-suited for analyzing these microstructures because it captures essential topological features—such as connected components, loops, and higher-dimensional voids—that conventional image-processing techniques often overlook. Previous studies have demonstrated PH's effectiveness in characterizing biological and physical systems with tree-like structures, including vascular networks and fracture propagation (https://homcloud.dev/) [31–33]. In the context of dendritic growth, PH provides a robust quantitative framework for tracking the formation and evolution of branches across multiple scales, thereby enabling the identification of structural transitions that influence growth mechanisms and stability. By integrating PH into our analysis, we gain deeper insights into the topological evolution of dendrites.

By leveraging PH in combination with machine learning-based Topological Data Analysis, we aimed to predict and classify various material properties effectively. In machine learning, we employed principal component analysis (PCA), which allows highly interpretable multivariate analysis[34]. PCA's advantage lies in its ability to extract essential features inherent in the data as basis vectors, enabling the visualization of distances and trends among data points in a low-dimensional space. The orthogonal nature of PCA's basis vectors preserves Euclidean distances, allowing us to analyze correlations between these distances and physical parameters without distorting the data space. Applying PCA to dendritic structures enabled us to comprehensively quantify and analyze structural changes in complex dendritic morphologies.

Building on the PCA results, we associated structural changes respect to Gibbs free energy to visualize and analyze the growth process within the data space. Since Euclidean distances are preserved within the PCA subspace, we

could quantitatively assess the total energy cost consumed by structural changes. This approach facilitated a robust connection between Gibbs free energy—which is crucial in crystal growth processes—and microstructure within the data space, providing deeper insights into the growth mechanisms of dendritic branching.

In our discussion, we perform correlation analyses between the extracted feature and physical parameters, providing physical interpretations of these features. Specifically, we analyze the gradient of Gibbs free energy to explore the conditions under which structural branching occurs. We attempt to extract hidden information embedded within complex dendritic growth processes. By synthesizing acquired insights, we deepen our understanding of the mechanisms governing dendrite growth. This series of analyses effectively utilizes image data to construct a data-driven functional analysis model. Furthermore, building on our proven track record in developing an "extended Landau free energy model" for magnetic materials [35–42], we expand this concept to incorporate Gibbs free energy. By applying the modeling techniques developed for closed systems in magnetic materials to open systems, we enhance the generality of the model. *[Fig. 1 near here]*

2 Methods

2.1 Input data preparation by phase field simulation

We generated input images of dendritic microstructure growth using phase-field simulations based on the Time-Dependent Ginzburg-Landau (TDGL) equation.

$$\frac{\partial \varphi}{\partial t} = -M \frac{\delta E_{total}}{\delta \varphi} \tag{1}$$

, where φ is the phase-field variable serving as the order parameter of the system. The mobility M is a material-specific parameter that describes the kinetics of the system's evolution. The term $\frac{\delta E_{total}}{\delta \varphi}$ is the derivative of the total free energy E_{total} respect to the order parameter φ. This derivative represents the driving force for crystal growth of the system. In this study, we employed a typical phase-field simulation. The computational procedures and parameters are provided in the supplementary material[19,43–45].

We varied the anisotropy strength γ and the conditions of the initial nuclei. The anisotropy strength refers to the magnitude of anisotropy in the interfacial energy. It is known that metallic materials form various microstructures depending on this anisotropy strength. To replicate these microstructures, we introduced directional dependence—namely, interfacial anisotropy—into parameters such as surface energy, interfacial energy, and grain boundary energy. Specifically, we set γ = 0.005, 0.015, and 0.025. For the initial nuclei, we prepared three types: circular, regular hexagonal, and square shapes. To establish fundamental principles, we conducted calculations with a size of 10 pixels, where the dependence on the initial nucleus is prominently manifested.

We conducted simulations on a grid size of 350 × 350 pixels, obtaining images as 8-bit grayscale data. Simulations were performed up to 30000 steps. In the dataset used for this study, we acquired a total of 301 images at intervals of every 100 steps, repeating the simulations three times under identical conditions to ensure reproducibility. The

dendritic structures were set to exhibit sixfold symmetry. Notably, the total free energy was not used in the machine learning process; only the images served as input for machine learning. The dataset employed in this study comprised five different anisotropy strengths, five levels of noise, and three types of initial nucleus shapes. To confirm reproducibility, simulations were conducted three times under each condition, generating 301 images per trial. In total, we prepared 67,725 images and used for machine learning.

2.2 Persistent homology analysis

We extracted the morphology of dendritic structures as feature using PH (Fig. 2) [25,27–29,35,40]. We applied filtration to binary data, where each pixel in the images stores either a 1 (white) or a 0 (black), corresponding to the presence or absence of material, respectively (Fig. 2(a)). In PH analysis, we calculated the distance transform for each pixel based on the Manhattan distance, using the boundaries between white and black pixels as reference points. By continuously varying the threshold values in the Manhattan distance, we expanded and contracted the boundary surfaces (Fig. 2(b)). During this process, we recorded the threshold b at which "holes" are created (birth) and the threshold d at which they disappear (death), thereby extracting structural features (Fig. 2(c)). The pairs (b, d), known as generators, serve as information characterizing the shapes of the holes. By processing these thresholds across the entire image, we constructed a persistence diagram (PD), which visually represents these fine structure (Fig. 2(d)).

For example, in stripe-like structures, the values of b and d are approximately equal, so generators appear along the diagonal of the PD (I and II). In bubble-like structures, generators appear in the upper region of the PD where $d > b$ (III and IV). Curved structures generate generators in distinct regions of the PD corresponding to their geometric properties (V). By processing the boundary movements in both positive and negative directions—thickening the structures in the positive case and thinning them in the negative case—we could describe not only the holes but also the connectivity of the structures. The PD encapsulates the structural information of the data, enabling quantitative analysis of microstructure morphology. By utilizing the distribution of (b, d)pairs that appear on the PD, we can effectively describe microstructures. In this study, we obtained feature vectors by applying Gaussian kernels and weighting functions to the acquired PDs. Furthermore, the generators in the PD can be inversely mapped to their corresponding original spatial coordinates, allowing us to trace back to the coordinate information in the original images. *[Fig. 2 near here]*

2.3 Dimensionally reduction by PCA

PCA is one of popular unsupervised machine learning and is a method used to reduce high-dimensional vectors $\{\boldsymbol{x_i} \,|x_1^i, \ldots, x_p^i\}$ to low-dimensional vectors $\{\boldsymbol{y_i} \mid \left(y_1^i, \ldots, y_m^i\right),\ m < p\}$ [34]. This technique involves constructing a projection matrix $\boldsymbol{W} = \{\boldsymbol{w}_1, \ldots, \boldsymbol{w}_i \mid \boldsymbol{w}_i = (w_1, \ldots, w_p)\}$ to compress the high-dimensional variance information into a lower-dimensional space while preserving as much of the original data variability as possible (Equation (1)).

$$\boldsymbol{y} = \boldsymbol{W}\boldsymbol{x}\#\#(1)$$

, where $\boldsymbol{x} = \{\boldsymbol{x_1}, \ldots, \boldsymbol{x_n}\}$, $\boldsymbol{y} = \{\boldsymbol{y_1}, \ldots, \boldsymbol{y_n}\}$. The vectors $\boldsymbol{w}_i$ constituting the projection matrix $\boldsymbol{W}$ are the basis vectors (PCA loadings), and the projected vectors $\boldsymbol{y_i} = (y_1^i, \ldots, y_m^i)$ are the principal components. Principal components are denoted sequentially from the first principal component as PC1, PC2, ..., PCm, with lower numbers indicating higher explainability. Specifically, we transformed the persistence diagrams (PDs) into vectors according to a positive-definite kernel and stacked the series of data from the dendritic growth process to create a large composite matrix. We then applied PCA to reduce the dimensionality from 3,240 dimensions to 2 dimensions. For the PCA analysis, we used data from steps 4,000 to 30,000. This approach is expected to visualize the complex structural changes in dendritic growth within a low-dimensional space. By analyzing the correlation between the extracted feature vectors and physical parameters, we determined the physical interpretation of these features. Additionally, we conducted correlation analyses focusing on Gibbs free energy to analyze the growth process and to gain insights into the underlying mechanisms.

3. Results and discussion

3.1 Input data

Figure 3 presents dendritic structures generated via phase-field simulations, which serve as the input data for our machine learning analysis. These simulations were conducted under varying anisotropy strengths (0.005, 0.015, and 0.025) and with different initial nucleus shapes (square, circular, and hexagonal), thereby providing a diverse dataset that captures the influence of both initial geometry and anisotropy on dendritic growth morphology.

For square nuclei, branching occurs consistently in the primary arms across all anisotropy strengths, with these branches persisting throughout the growth process (Fig. 3a). The pronounced effect of the square nucleus is evident in the robust and stable branching observed in the primary arms. In the case of circular nuclei, branching also appears in the primary arms (Fig. 3b); however, its stability is dependent on the anisotropy strength. At a low anisotropy of 0.005, the branches remain prominent throughout the growth process, whereas at higher anisotropy levels (0.015 and 0.025), the branches become less stable and gradually merge, leading to smoother structures. For hexagonal nuclei, dendritic growth progresses symmetrically without any branching in the primary arms, regardless of the anisotropy strength (Fig. 3c). The resulting structures maintain a sixfold symmetry, reflecting a smooth and uninterrupted pattern of crystal growth. Overall, Figure 3 underscores the diverse dendritic growth behaviors governed by physical parameters such as initial nucleus shape and anisotropy, thereby illustrating the relationship between these factors and the morphological evolution of the structures. Thus, we were able to visually confirm the complex morphological changes in the dendritic structures.

[Fig. 3 near here]

3.2 Characterization of dendrite morphology by PH

The morphological features of dendritic structures were extracted using persistent homology (PH) and vectorized as persistence diagrams (PDs) (Fig. 4). In these diagrams, the generators are distributed in regions slightly offset from the diagonal, thereby capturing distinct structural characteristics of the dendritic growth process. As the dendritic structures evolve, the generators systematically shift toward the lower right in the PDs, corresponding to specific microstructural features (see the supplementary movie).

To establish a direct correspondence between the PD and the dendritic morphology, the generators in the PD are mapped back to the original images as red dots. In Fig. 4, generators located around (-30, -28) represent the thickest primary arms, those near (-20, -18) correspond to moderately thick primary arms with branching, and those around (-8, -6) capture the finer secondary arms. This clear segregation demonstrates that the PDs effectively distinguish the branching characteristics inherent in dendritic morphology. Furthermore, the distribution of PD generators reflects the influence of the initial nucleus shape. For square and circular initial nuclei (Figs. 4a and 4b), where branching occurs in the primary arms, generators are densely clustered around (-20, -18), effectively capturing the features of the branched primary arms. In contrast, for hexagonal initial nuclei (Fig. 4c), which naturally lack branching in the primary arms, the PDs exhibit significantly fewer generators near (-20, -18). This absence is consistent with the unbranched morphology observed in the hexagonal configuration. These findings underscore the effectiveness of persistence diagrams in capturing the morphological features of dendrites—particularly their branching behavior—and demonstrate the robustness of persistent homology across varying initial conditions.

The statistical stability of persistence diagrams (PDs) is a crucial element in topological data analysis. Previous studies have demonstrated that persistent homology (PH) provides a robust framework for characterizing structured patterns, such as magnetic domains [46]. For instance, PDs generated from domain patterns with identical macroscopic magnetic states—but with varying microstructures—exhibited remarkably consistent profiles, yielding an average cosine similarity of 0.992. In contrast, when an external magnetic field induced simultaneous changes in both macroscopic and microstructural properties, the similarities between PDs varied widely (ranging from 0.2 to 1), reflecting the underlying transformations. These results confirm that PH effectively captures microstructural variations while maintaining statistical consistency, thereby underscoring its reliability for analyzing dendritic growth and identifying structural changes during crystal growth processes.

[Fig. 4 near here]

3.3 Visualization of the energy landscape in data space

We performed dimensionality reduction using Principal Component Analysis (PCA) (Fig. 5). Since the evolution data of the PDs constitutes a high-dimensional dataset, we compressed it into a low-dimensional space with PCA. Applying PCA to the matrix constructed from the PDs yielded two eigenvectors, PC1 and PC2, which represent the complex changes in the PDs. Each point in the scatter plot represents an image, with the symbols indicating the initial nucleus shapes and the anisotropy strength also noted. The coordinates of the scatter plot are the PC1 score and PC2 score, and the distance of the points corresponds to changes in the images. The PCA results represent the continuous evolution of dendritic growth mapped onto a two-dimensional plane. Furthermore, because each point is associated with the total energy, we can analyze the relationship between image changes and changes in total energy. Particularly, since Euclidean distances are preserved within the PCA subspace, we can quantitatively analyze the total energy cost consumed by structural changes. In other words, this figure illustrates the relationship between the structural evolution and the total energy, effectively representing the correspondence between structure and process (system stability) in a single comprehensive diagram. *[Fig. 5 near here]*

3.4 Energy analysis in data space

Through the correlation analysis between the obtained features and physical properties, we discussed detailed insights into the dendritic growth process (Fig. 6). The total energy E_{total}, as defined in Sect. 2.1 (Eq. 1), is used for analyzing the relationship between morphological evolution and free energy. We observed that PC1 increased and total energy monotonically decreased with the growth of dendritic structures (Fig. 6(a)). Notably, total energy E_{total}—a key physical quantity in the dendrite growth process—exhibited a clear correlation with PC1. It indicates that PC1 is a useful feature representing both dendritic growth and total energy. Moreover, we confirmed a distinct kink around PC1 ≈ -1, where a sudden decrease in total energy occurs.

We then examined the physical interpretation of PC2 (Fig. 5). The sign of PC2 corresponds to the presence and absence of branching in the primary arms. Importantly, this distinction remains consistent regardless of anisotropy strength or initial nucleus shape, suggesting that PC2 serves as a useful feature for characterizing branching in complex dendritic growth. Further analysis is required to interpret the physical significance of PC2. *[Fig. 6 near here]*

Since the region where branching occurs corresponds precisely to the kink in the Total Energy vs. PC1, we focused on this area to perform a detailed analysis of the energy gradient (Fig. 6(b)). Given that PC1 was a useful feature representing morphological growth, we differentiated the total energy with respect to PC1. [31, 33]

By analyzing the energy gradient within the data space [35,37], we were able to manifest kink in the total energy as an outlier. In systems where the total energy decreases monotonically without a kink, the branching of the primary arms does not fill in, and the structure continues to grow as is. In systems with a kink, the branching of the primary arms fills in early, and the sixfold symmetrical structure growth progresses smoothly. It is considered that filling in the branches reduces the total energy, stabilizes the system, and promotes the growth of a highly symmetrical crystal. Linear dimensionality reduction with energy outlier analysis may have uncovered nonlinear behavior.

We aim to deepen the discussion regarding the physical interpretation of the gradient analysis results. In the TDGL equation, the gradient of total free energy E_{total} with respect to the order parameter φ (structure) is defined as the driving force as described in equation (1). In our analysis, the gradient involves differentiating the total free energy with respect to structural features extracted by PH, thereby treating the driving force from a data science perspective. We here refer to this quantity, which encapsulates information about the driving force, as the "feature-extended driving force". In system with a monotonous gradient, the feature-extended driving force changes monotonously, indicating smooth thin-film growth occurs. Conversely, in systems where the gradient varies, the feature-extended driving force also changes, suggesting discontinuous crystal growth. In other words, this captures changes in the acceleration of crystal growth, and indeed, variations in the gradient correspond to branch filling (Fig. 6(b)). Such energy gradient data analysis would offer the discussion of the underlying mechanisms in growth process.

Furthermore, the coordinates where branching occurs were almost identical regardless of the initial nucleus shape or anisotropy strength. This suggests that we have obtained an useful feature applicable to various materials. The coordinates of PC1 and PC2 may represent a distinct phase boundary that governs branching. In other words, we have acquired useful features that lead to flat thin-film growth.

In this study, we establish the relationship between structure and process in dendritic growth using explainable

machine learning approaches. By employing PH, we quantitatively described the morphology of dendritic structures. Additionally, we used highly interpretable dimensionality reduction techniques to robustly construct the relationship between structural changes and free energy within the data space. Specifically, by thoroughly analyzing the relationship between Gibbs free energy and the morphological evolution of dendrites, we elucidated the growth mechanisms of dendritic branching. As a result, we obtained useful features PC1 and PC2 determining the branching, and new insights into flat thin film growth. This model would generalize the concept of the extended Landau free energy, which we previously developed for magnetic materials, from a closed system to an open system[35–37,39–41].

Our method offers a versatile approach to material analysis. For instance, in two-dimensional materials such as CVD graphene, borophene, and silicene [8,9,14,15,21], defects are incorporated as network structures, enabling the analysis of their atomic-scale geometric configurations[15,47]. Additionally, free energy serves as a critical physical property that characterizes various functionalities, including oscillation characteristics and power consumption in applied device. This capability facilitates a hierarchical connection between atomic-scale microstructures and macroscopic functionalities, paving a way for future advancements.

Moreover, by leveraging the versatility of thermodynamic concepts, we can integrate various energy terms into free energy. For example, conducting multiphysics analyses of interactions between electrons and forces opens up possibilities for sensor applications. Notably, our expertise in analyzing magnetostriction—where magnetization and strain interact—demonstrates the effectiveness of our approach [38]. Consequently, we anticipate establishing a robust hierarchical connection between structure and function across a wide range of applied materials.

Fundamentally, energy landscape analysis within data spaces could lead to advancements in nonequilibrium physics. Analyzing the stability and dynamics of energy landscapes could present excellent research opportunities [27]. Additionally, incorporating nonlinear dimensionality reduction techniques may facilitate the analysis of nonlinear phenomena. Specifically, latent features such as PC2 obtained in this study have the potential to uncover knowledge that was previously inaccessible. Utilizing data science could help organize and resolve some of the challenges associated with complex systems. Thus, the fusion of mathematics and physics is anticipated to drive diverse developments, ranging from fundamental research to practical applications.

Acknowledgements

This work was supported by the Japan Science and Technology Agency (JST) CREST (Grant No. JPMJCR21O4). This work was partially supported by the Japan Society for the Promotion of Science (KAKENHI) Grant-in-Aid for Scientific Research (A) (21H04656), Grant-in-Aid for Challenging Research (Exploratory) (19K22117) and Beyond 5G Research and Development Project (grant number:05901), and JST-Mirai Program (grant number: JPMJMI22708192). We thank to Prof. K. Akagi, Prof. T. Nakamura and Prof. K. Ono for useful discussions. We gratefully acknowledged Prof. Fukuyama for his thoughtful discussions and expert guidance, which have been instrumental in shaping the direction and depth of this study.

Disclosure statement

The authors declare that there are no conflicts of interest regarding the publication of this paper. No competing financial or non-financial interests are involved in the research, authorship, and publication of this work.

Data availability statement

The data that support the findings of this study are available from the corresponding author upon reasonable request.

Reference

[1] Romagnoli M, Sorianello V, Midrio M, et al. Graphene-based integrated photonics for next-generation datacom and telecom. Nat Rev Mater. 2018;3(10):392–414.

[2] Li M-Y, Su S-K, Wong H-SP, et al. How 2D semiconductors could extend Moore's law. Nature. 2019;567(7747):169–170.

[3] Endoh N, Akiyama S, Tashima K, et al. High-Quality Few-Layer Graphene on Single-Crystalline SiC thin Film Grown on Affordable Wafer for Device Applications. Nanomaterials. 2021;11(2):392.

[4] Akinwande D, Huyghebaert C, Wang C-H, et al. Graphene and two-dimensional materials for silicon technology. Nature. 2019;573(7775):507–518.

[5] Liu Y, Duan X, Shin H-J, et al. Promises and prospects of two-dimensional transistors. Nature. 2021;591(7848):43–53.

[6] Nishiguchi K, Yamaguchi H, Fujiwara A. Subgigahertz Multilayer-Graphene Nanoelectromechanical System Integrated with a Nanometer-Scale Silicon Transistor Driven by Reflectometry. Phys Rev Appl. 2023;19(1):L011003.

[7] Fukidome H, Takahashi R, Abe S, et al. Control of epitaxy of graphene by crystallographic orientation of a Si substrate toward device applications. J Mater Chem. 2011;21(43):17242.

[8] Fukamachi S, Solís-Fernández P, Kawahara K, et al. Large-area synthesis and transfer of multilayer hexagonal boron nitride for enhanced graphene device arrays. Nat Electron. 2023;6(2):126–136.

[9] Dean CR, Young AF, Meric I, et al. Boron nitride substrates for high-quality graphene electronics. Nat Nanotechnol. 2010;5(10):722–726.

[10] Dolleman RJ, Belardinelli P, Houri S, et al. High-Frequency Stochastic Switching of Graphene Resonators Near Room Temperature. Nano Lett. 2019;19(2):1282–1288.

[11] Koh S, Kosuga S, Suga R, et al. Graphene transparent antennas. Carbon Reports. 2023;2(1):020104.

[12] Ono M, Hata M, Tsunekawa M, et al. Ultrafast and energy-efficient all-optical switching with graphene-loaded deep-subwavelength plasmonic waveguides. Nat Photonics. 2020;14(1):37–43.

[13] Suzuki S, Sekine Y, Kumakura K. Terahertz spectroscopy of graphene complementary split ring resonators with gate tunability. Jpn J Appl Phys. 2017;56(9):095102.

[14] Yoshioka K, Wakamura T, Hashisaka M, et al. Ultrafast intrinsic optical-to-electrical conversion dynamics in a graphene photodetector. Nat Photonics. 2022;16(10):718–723.

[15] Cuong NT, Tateishi I, Cameau M, et al. Topological Dirac nodal loops in nonsymmorphic hydrogenated monolayer boron. Phys Rev B. 2020;101(19):195412.

[16] Endoh N, Akiyama S, Tashima K, et al. High-Quality Few-Layer Graphene on Single-Crystalline SiC thin Film Grown on Affordable Wafer for Device Applications. Nanomaterials. 2021;11(2):392.

[17] Hasegawa M, Tashima K, Kotsugi M, et al. Inhomogeneous longitudinal distribution of Ni atoms on graphene induced by layer-number-dependent internal diffusion. Appl Phys Lett. 2016;109(11).

[18] Li X, Magnuson CW, Venugopal A, et al. Large-Area Graphene Single Crystals Grown by Low-Pressure Chemical Vapor Deposition of Methane on Copper. J Am Chem Soc. 2011;133(9):2816–2819.

[19] Kobayashi R. Modeling and numerical simulations of dendritic crystal growth. Physica D. 1993;63(3–4):410–423.

[20] Yan Z, Lin J, Peng Z, et al. Toward the Synthesis of Wafer-Scale Single-Crystal Graphene on Copper Foils. ACS Nano. 2012;6(10):9110–9117.

[21] Fukidome H, Kotsugi M, Nagashio K, et al. Orbital-specific Tunability of Many-Body Effects in Bilayer Graphene by Gate Bias and Metal Contact. Sci Rep. 2014;4(1):3713.

[22] Nagamura N, Konno S, Matsumoto M, et al. Photoelectron spectromicroscopy analysis of graphene during gate-controlled photo-oxidation process. Nano Express. 2022;3(4):044003.

[23] Ohkochi T, Takahashi R, Fujiwara H, et al. Investigation of deterministic and cumulative nature in helicity-dependent optical switching of ferrimagnetic Gd–Fe–Co films. J Magn Magn Mater. 2024;593:171854.

[24] Ohtsuki T, Kojima T, Kotsugi M, et al. Magnetic domain observation of FeCo thin films fabricated by alternate monoatomic layer deposition. J Appl Phys. 2014;115(4):043908.

[25] Obayashi I, Hiraoka Y, Kimura M. Persistence diagrams with linear machine learning models. J Appl Comput Topol. 2018;1(3–4):421–449.

[26] Edelsbrunner, Letscher, Zomorodian. Topological Persistence and Simplification. Discrete Comput Geom. 2002;28(4):511–533.

[27] Hiraoka Y, Nakamura T, Hirata A, et al. Hierarchical structures of amorphous solids characterized by persistent homology. Proceedings of the National Academy of Sciences. 2016;113(26):7035–7040.

[28] Minamitani E, Obayashi I, Shimizu K, et al. Persistent homology-based descriptor for machine-learning potential of amorphous structures. J Chem Phys. 2023;159(8).

[29] Kimura M, Obayashi I, Takeichi Y, et al. Non-empirical identification of trigger sites in heterogeneous processes using persistent homology. Sci Rep. 2018;8(1):3553.

[30] Hirata A, Wada T, Obayashi I, et al. Structural changes during glass formation extracted by computational homology with machine learning. Commun Mater. 2020;1(1):98.

[31] Li D, Nguyen P, Zhang Z, et al. Tree representations of brain structural connectivity via persistent homology. Front Neurosci. 2023;17.

[32] Nicponski J, Jung J-H. Topological Data Analysis of Vascular Disease: A Theoretical Framework. Front

Appl Math Stat. 2020;6.

[33] Li Y, Wang D, Ascoli GA, et al. Metrics for comparing neuronal tree shapes based on persistent homology. PLoS One. 2017;12(8):e0182184.

[34] Jolliffe I. Principal Component Analysis. International Encyclopedia of Statistical Science. Berlin, Heidelberg: Springer Berlin Heidelberg; 2011. p. 1094–1096.

[35] Kunii S, Masuzawa K, Fogiatto AL, et al. Causal analysis and visualization of magnetization reversal using feature extended landau free energy. Sci Rep. 2022;12(1):19892.

[36] Foggiatto AL, Kunii S, Mitsumata C, et al. Feature extended energy landscape model for interpreting coercivity mechanism. Commun Phys. 2022;5(1):277.

[37] Kunii S, Foggiatto AL, Mitsumata C, et al. Super-hierarchical and explanatory analysis of magnetization reversal process using topological data analysis. Science and Technology of Advanced Materials: Methods. 2022;2(1):445–459.

[38] Foggiatto AL, Mizutori Y, Yamazaki T, et al. Visualization of the Magnetostriction Mechanism in Fe-Ga Alloy Single Crystal Using Dimensionality Reduction Techniques. IEEE Trans Magn. 2023;59(11):1–4.

[39] Mitsumata C, Foggiatto AL, Kotsugi M. A Data-Driven Extended Landau Theory Method for the Coercivity Analysis of Magnetic Materials. 2024 IEEE International Magnetic Conference - Short papers (INTERMAG Short papers). IEEE; 2024. p. 1–2.

[40] Nagaoka R, Masuzawa K, Taniwaki M, et al. Quantification of the Coercivity Factor in Soft Magnetic Materials at Different Frequencies Using Topological Data Analysis. IEEE Trans Magn. 2024;60(9):1–5.

[41] Taniwaki M, Alexandre FL, Mitsumata C, et al. Analysis of Magnetization Reversal Process of Non-Oriented Electromagnetic Steel Sheet by Extended Landau Free Energy Model. 2023 IEEE International Magnetic Conference - Short Papers (INTERMAG Short Papers). IEEE; 2023. p. 1–2.

[42] Foggiatto AL, Nagaoka R, Taniwaki M, et al. Analysis of the Excess Loss in High-Frequency Magnetization Process Through Machine Learning and Topological Data Analysis. IEEE Trans Magn. 2024;60(9):1–5.

[43] Koyama T, Ohno M, Yamanaka A, et al. Development of Microstructure Simulation System in SIP-Materials Integration Projects. Mater Trans. 2020;61(11):2047–2051.

[44] Yamanaka A, McReynolds K, Voorhees PW. Phase field crystal simulation of grain boundary motion, grain rotation and dislocation reactions in a BCC bicrystal. Acta Mater. 2017;133:160–171.

[45] Warren JA, Boettinger WJ. Prediction of dendritic growth and microsegregation patterns in a binary alloy using the phase-field method. Acta Metallurgica et Materialia. 1995;43(2):689–703.

[46] YAMADA T, SUZUKI Y, MITSUMATA C, et al. Visualization of Topological Defect in Labyrinth Magnetic Domain by Using Persistent Homology. Vacuum and Surface Science. 2019;62(3):153–160.

[47] Tsujikawa Y, Zhang X, Yamaguchi K, et al. Quasi-Periodic Growth of One-Dimensional Copper Boride on Cu(110). Nano Lett. 2024; doi: 10.1021/acs.nanolett.3c03861.

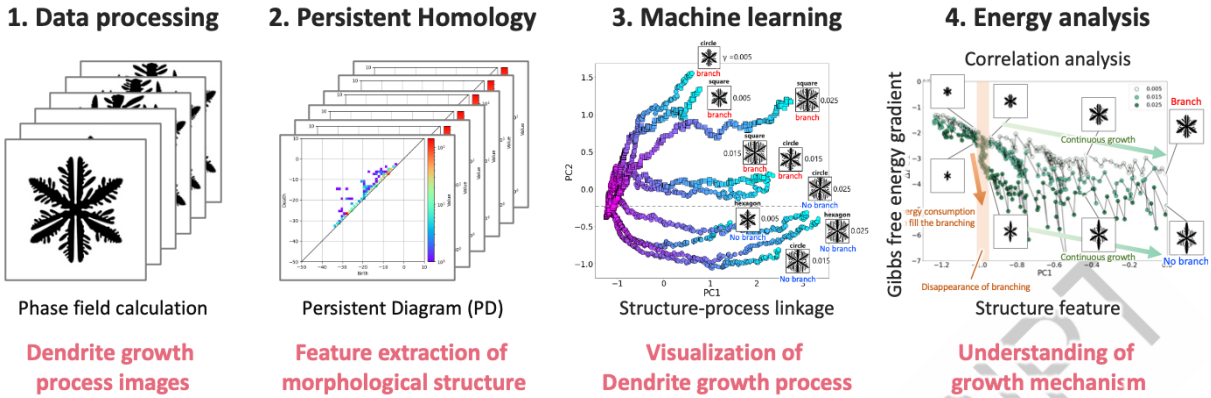

Fig. 1. Workflow of this study: Hierarchical connection between structure and process in dendritic growth using data science approach.

We generated large-scale data of dendritic structures using phase-field simulations. The morphology of the dendrites was extracted as features using persistent homology. Utilizing unsupervised machine learning, we visualized the dendritic growth process in a low-dimensional space. This approach allowed us to construct the relationship between structure and process. By analyzing the correlations between free energy and structural features, we elucidated the branching mechanisms in dendritic growth.

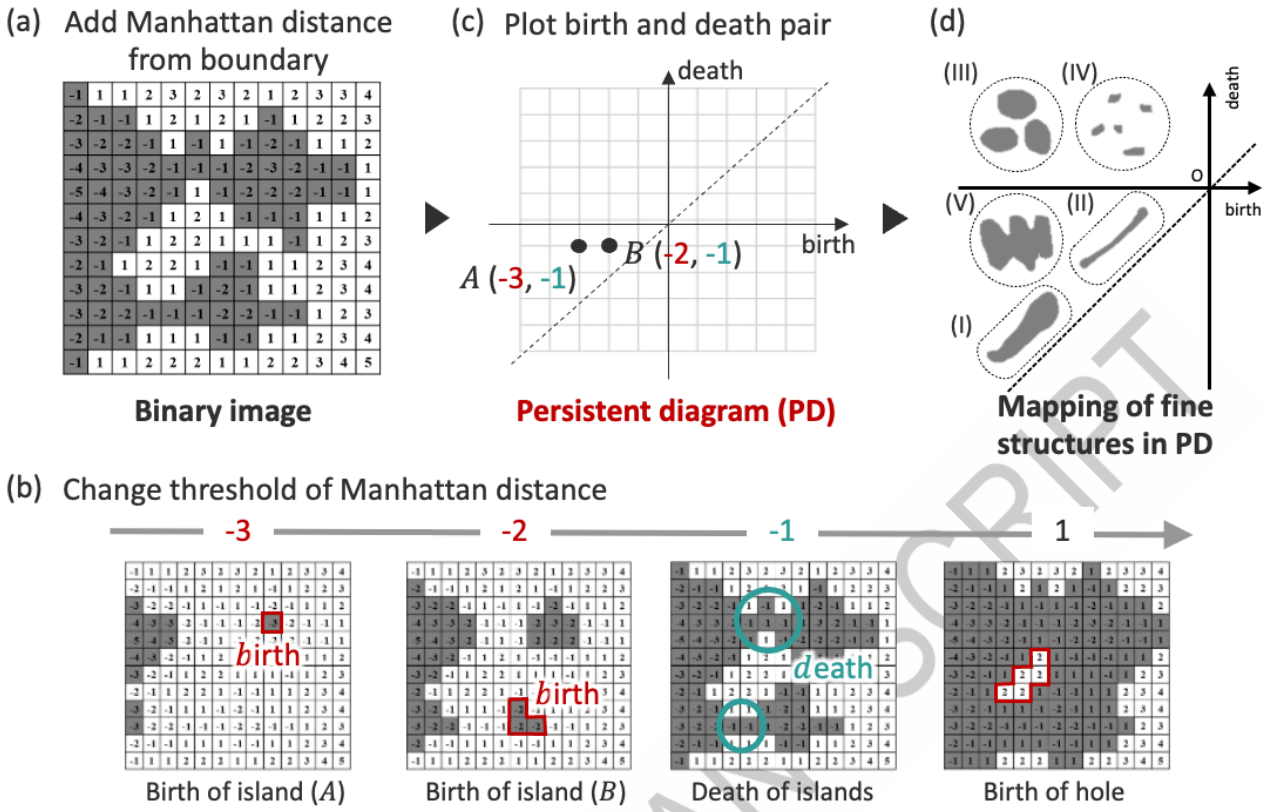

Fig.2 Persistent Homology analysis

To characterize the morphology of dendrite, we begin with binarized input images where each pixel is assigned a Manhattan distance index from the boundary (a). By systematically varying the distance threshold, we identify the points at which islands emerge (birth) and merge (death) (b). These birth and death events are then used to construct a persistence diagram (PD) (c). The PD effectively captures the connectivity of the islands and the presence of voids or holes within the structure. PD describes the fine structural patterns, such as bubbles, stripes, and constricted shapes, as depicted in a schematic diagram (d).

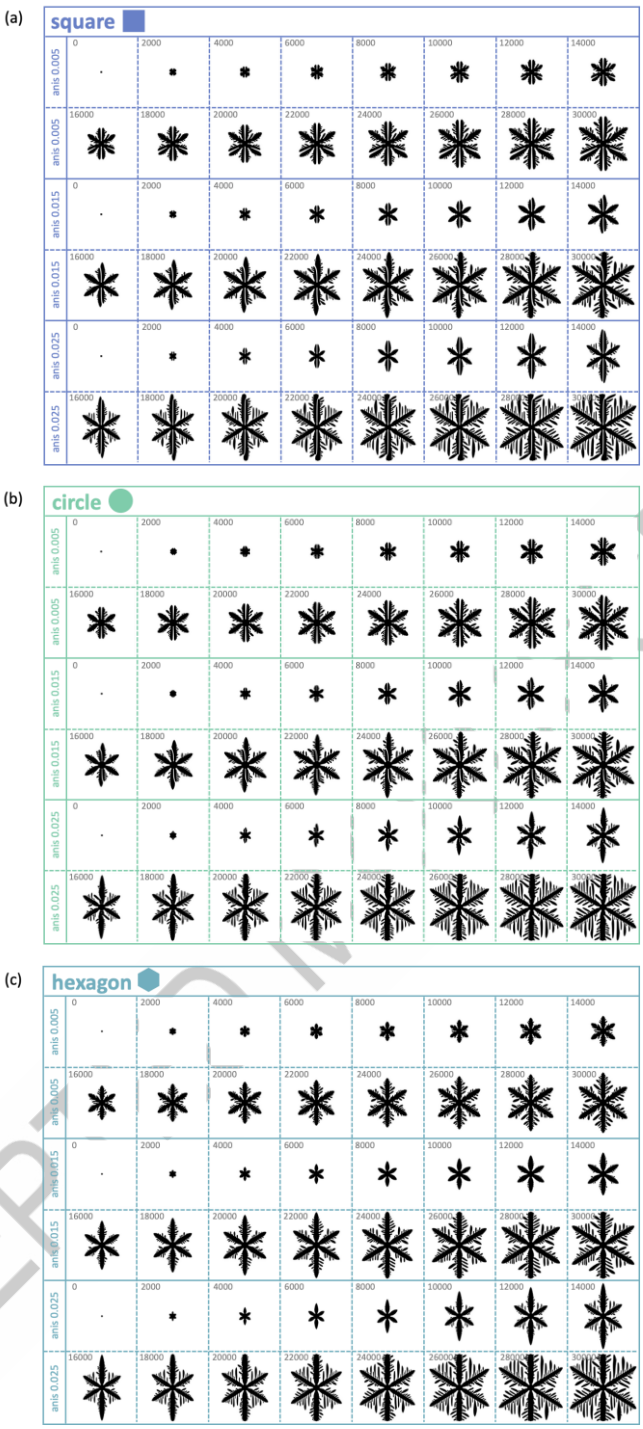

Fig. 3. Dendritic structures generated via phase-field simulations under varying initial nucleus shapes and anisotropy strengths.

(a) Square nuclei exhibit consistent primary arm branching across all anisotropy strengths, with branches persisting throughout growth. (b) Circular nuclei also produce primary arm branching, but its stability decreases with higher anisotropy, leading to smoother final structures. (c) Hexagonal nuclei result in symmetric, branch-free dendritic growth, maintaining sixfold symmetry regardless of anisotropy. These simulations illustrate the influence of initial geometry and anisotropy on dendritic morphology, providing input data for machine learning analysis.

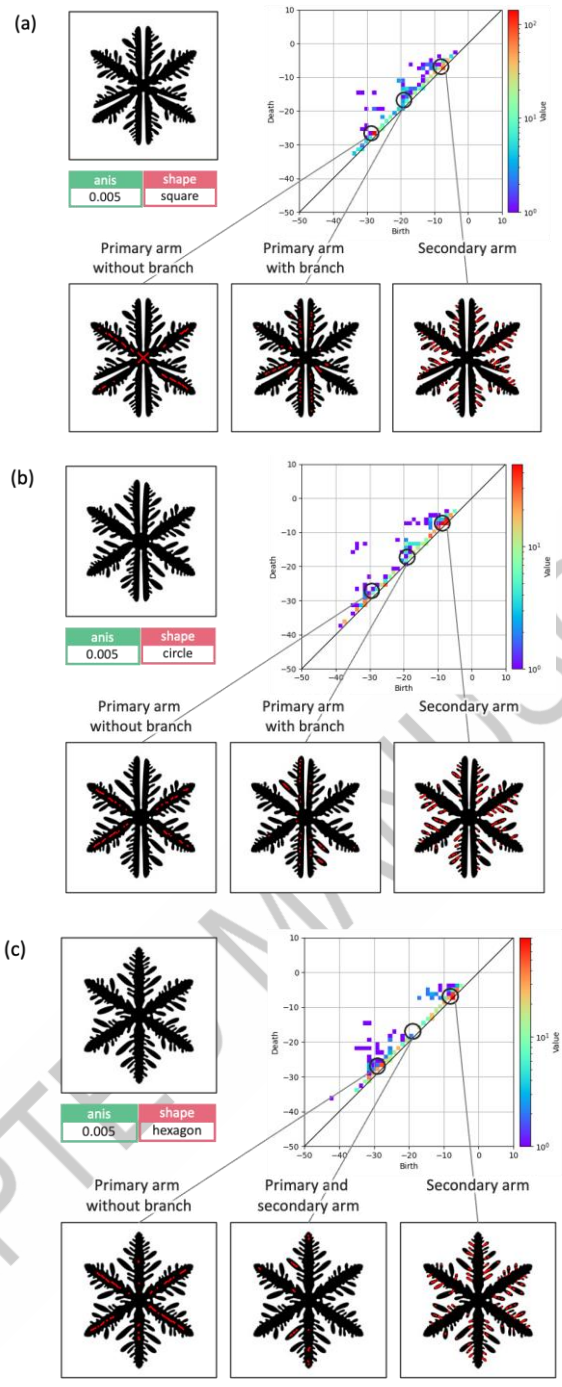

Fig. 4. Relationship Between the Persistence Diagram (PD) and the Morphology of Dendritic Structures. Generators in the PDs are systematically distributed, shifting towards the lower right as thickness of dendrite arm. Generators around (-30, -28) correspond to the thickest primary arms, those near (-20, -18) represent branched primary arms, and those around (-8, -6) capture secondary arms. The PD distributions also reflect the influence of initial nuclei, with square (a) and circular (b) nuclei showing dense generators near (-20, -18) due to branching, while hexagonal nuclei (c) exhibit fewer generators in this region, aligning with their unbranched morphology. These results demonstrate the effectiveness of PH in characterizing dendritic growth and structural variations.

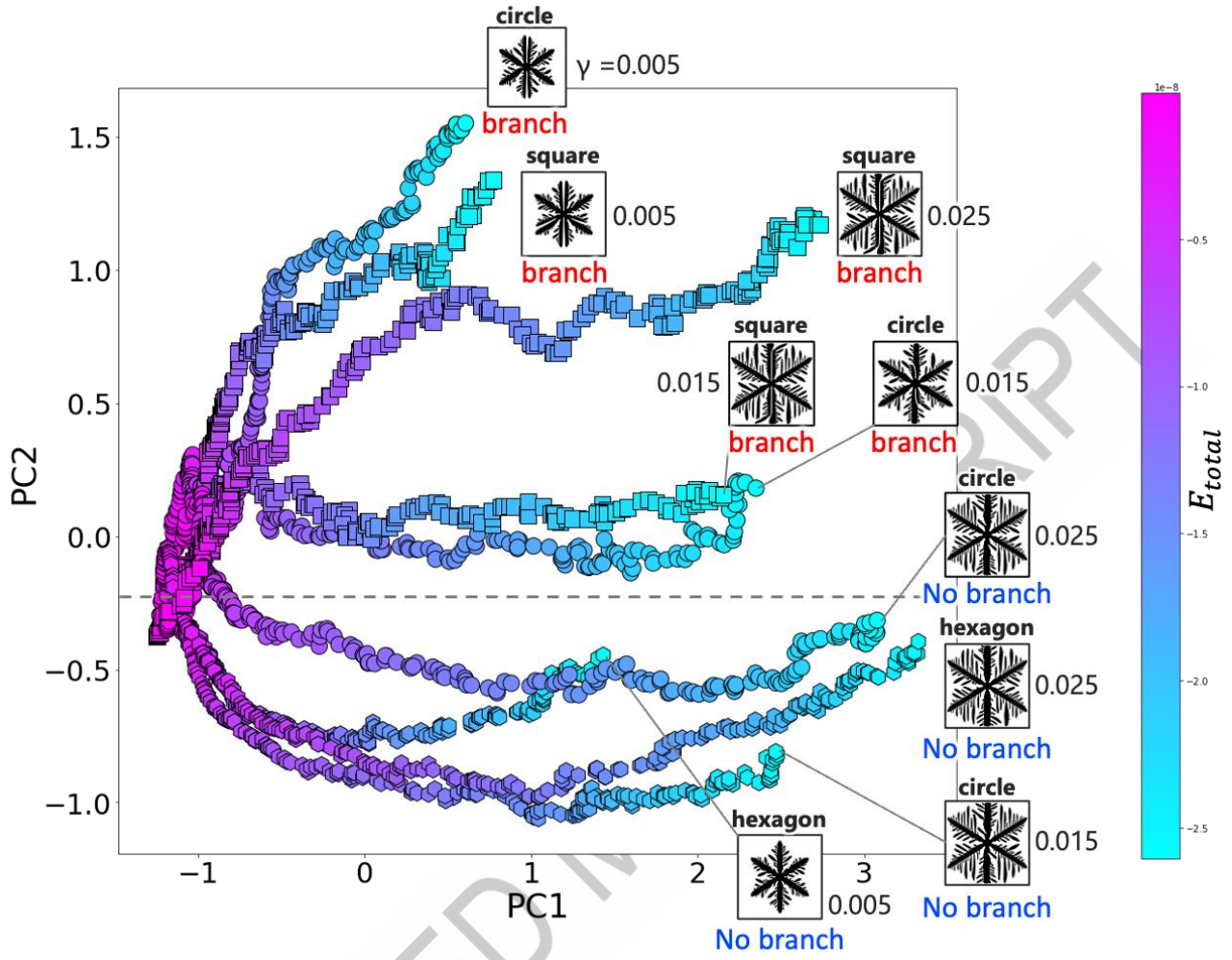

Fig. 5. Results of Dimensionality Reduction Using PCA

Each point represents an image, and the distance of data points corresponds to the microstructure changes. Each point is also associated with its Gibbs free energy. By visualizing the changes in energy consumed during structural growth, we established the relationship between structure and process. It is confirmed that the PC1 score shows clear correlation with growth evolution and the total energy, while PC2 is a feature that determines the presence and absence of branching in primary arm.

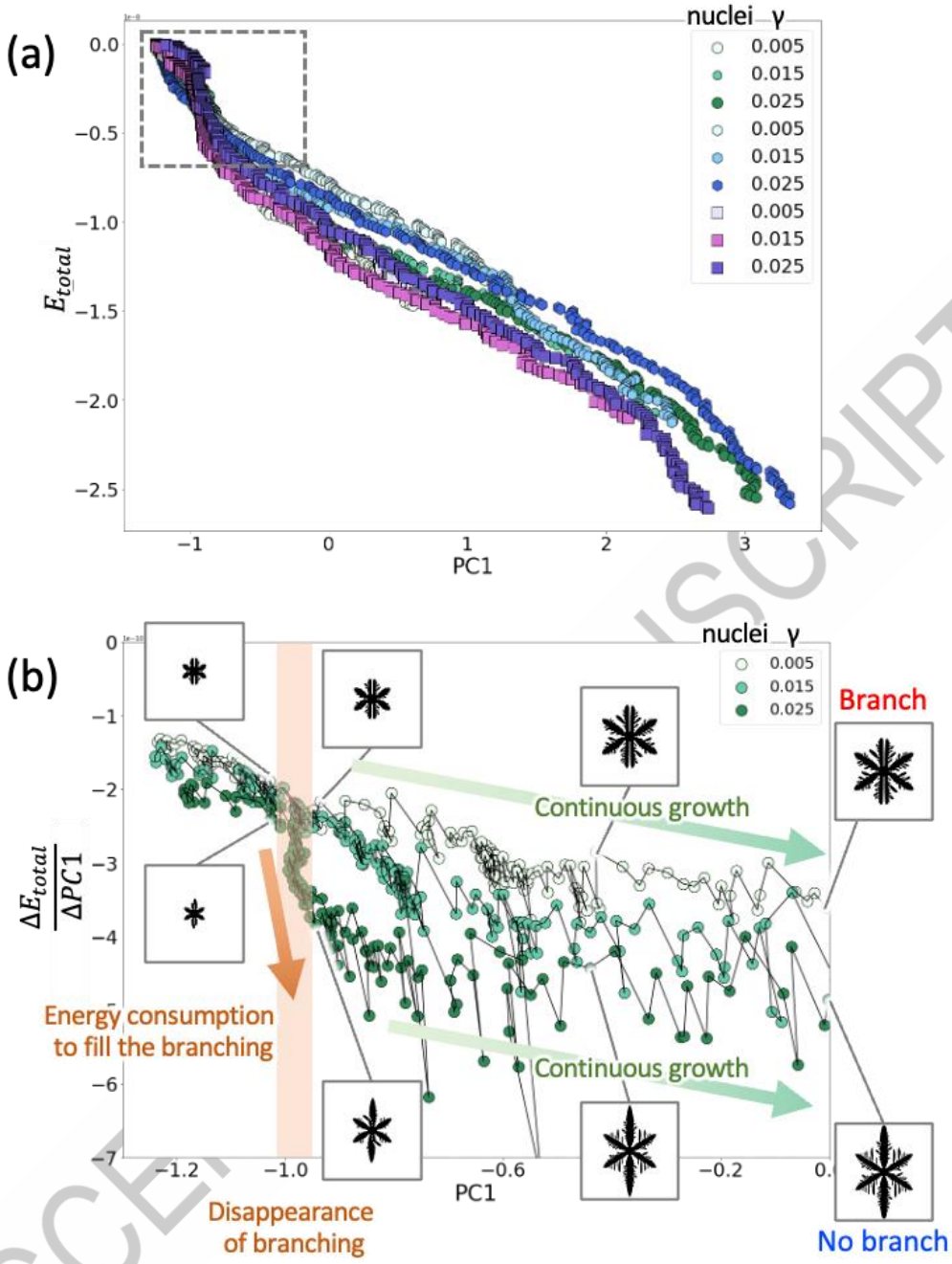

Fig. 6. (a) Correlation Between PC1 and Total Energy.

PC1 increased and total energy monotonically decreased with the growth of dendritic structures. A clear correlation indicates that PC1 is a useful feature representing both dendritic growth and total energy. Although energy variations are mostly linear, a kink is observed near PC1 ≈ -1. (b) To analyze around the kink in detail, we differentiated the total energy with respect to PC1 to examine the energy gradient. As a result, we found that the system consumes total energy to fill in the primary arms, after which the system stabilizes and promotes the growth of a highly symmetrical structure.

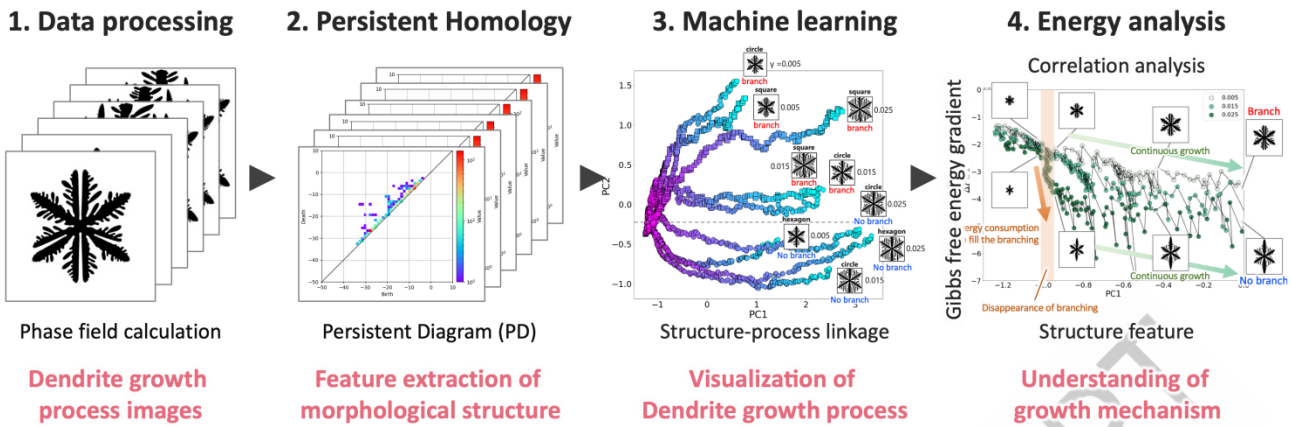

Graphicalabstract

Statement of novelty

We introduce a novel method that bridges structure and process in dendritic growth by integrating persistent homology with energy analysis. Our framework quantitatively maps dendritic morphology to Gibbs free energy variations, revealing energy gradients that drive branching behavior. This approach provides new insights into crystal growth and offers a powerful, data-driven pathway for optimizing thin-film fabrication.

Supplementary material

1. Phase-Field Method and Free Energy

1.1. Phase-Field Method and Free Energy

The phase-field method is employed to simulate the evolution of microstructures during phase transitions by minimizing the total free energy F of the system. This free energy is a combination of different contributions, represented as

$$F = \int_V \left[f_{chem}(\varphi) + f_{grad}\left(\nabla\varphi\right) + f_{doub}(\varphi) \right] dV$$

f_{chem} is the chemical free energy, which depends on the composition of the phases in the system. f_{grad} is the gradient energy, capturing the energetic cost associated with spatial variations in the phase field variable. f_{doub} is the double well energy, which stabilizes the phase field variable at specific values. The phase field variable φ represents the state of the material, varying between 0 and 1, where 0 corresponds to the solid phase and 1 to the liquid phase.

The phase-field evolution is governed by the Allen-Cahn equation,

$$\frac{\partial \varphi}{\partial t} = -M \frac{\delta F}{\delta \varphi}$$

, where M denotes the mobility and $\frac{\delta F}{\delta \varphi}$ is the variational derivative of the free energy, acting as the driving force for phase changes.

1.2. Anisotropy and Dendritic Growth

Anisotropy strength γ is a key factor in shaping the morphology of dendritic growth. It modulates the interface energy, affecting the directional dependence of interface dynamics. In this study, anisotropy is expressed as

$$\gamma(\theta) = \gamma_0 \left(1 + \epsilon \cos(n\,\theta)\right)$$

, where $\gamma_0$is the isotropic interface energy, ϵ represents the anisotropy strength, and nnn controls the anisotropic symmetry. Higher anisotropy strength ϵ leads to more pronounced directional growth, resulting in well-defined dendritic structures.

The development of dendritic structures is governed by the interplay between thermal diffusion and the phase field dynamics, described by the temperature equation and the phase field equation, respectively.

The temperature field in the solidifying material is modeled by the heat conduction equation,

$$\frac{\partial T}{\partial t} = \alpha \nabla^2 T + L\frac{\partial \varphi}{\partial t}$$

, where T is the temperature, t is time, α is the thermal diffusivity, L is the latent heat of fusion.
To solve numerically, the Allen-Cahn equation can be approximated to[S1,S2]

$$\frac{\partial \phi}{\partial t} = M\left[\nabla\left(\gamma_0{}^2\nabla\phi\right) - \frac{\partial}{\partial x}\left(\gamma_0\frac{\partial a}{\partial \theta}\frac{\partial \phi}{\partial y}\right) + \frac{\partial}{\partial y}\left(\gamma_0\frac{\partial a}{\partial \theta}\frac{\partial \phi}{\partial x}\right) + 4W\phi(1-\phi)\left(\phi - 0.5 - \frac{15}{2W}\frac{L(T-T_m)}{T_m}\phi(1-\phi) + \xi\right)\right]$$

where x and y are spatial coordinates, γ_0 is the anisotropy strength, W is the double well potential, T_m is the melting temperature, and ξ represents noise or fluctuations in the system that can influence the phase transition.
And the heat conduction equation

$$\frac{\partial T}{\partial t} = \kappa\nabla^2 T + 30\phi^2(1-\phi)^2\frac{L}{c}\frac{\partial \phi}{\partial t}$$

where κ is the thermal diffusivity, and c is the specific heat capacity. The term $30\phi^2(1-\phi)^2$ accounts for the contribution of the phase transition to the heat flow, ensuring that the release or absorption of latent heat is properly incorporated into the temperature evolution.
The parameters used for the simulation are displayed bellow:

Melting point T_m	$1728\ K$
Temperature of supercooled liquid T_O	$1511.2\ K$
Thermal conductivity K	$84.01\ W \cdot m^{-1} \cdot K^{-1}$
Specific heat C_p	$5.42 \times 10^6\ J \cdot K^{-1} \cdot m^{-3}$
Latent heat L	$2.35 \times 10^9\ J \cdot m^{-3}$
Interfacial kinetic coefficient μ	$2.0\ m \cdot K^{-1}s^{-1}$
Difference block length Δx	$30\ nm$
Interfacial width δ	$\delta = 3\Delta x\ nm$

[S1] J.A. Warren and W. J. Boettinger, Acta Metall. Mater., 43 (1995), p. 689
[S2] T. Takaki and A. Yamanaka, Phase-field method, Yokendo-Ltd., (2012), Section 5.3 (in Japanese)